Chemical Science

ROYAL SOCIETY OF CHEMISTRY

EDGE ARTICLE

View Article Online
View Journal | View Issue

Cite this: *Chem. Sci.*, 2021, **12**, 14230

All publication charges for this article have been paid for by the Royal Society of Chemistry

Noria and its derivatives as hosts for chemically and thermally robust Type II porous liquids†

Francesca M. Alexander,[a] Sergio F. Fonrouge,[b] José L. Borioni,[b] Mario G. Del Pópolo,[b] Peter N. Horton,[c] Simon J. Coles,[c] Benjamin P. Hutchings,[a] Deborah E. Crawford[d] and Stuart L. James *[a]

Porous Liquids (PLs) are a new class of material that possess both fluidity and permanent porosity. As such they can act as enhanced, selective solvents and may ultimately find applications which are not possible for porous solids, such as continuous flow separation processes. Type II PLs consist of empty molecular hosts dissolved in size-excluded solvents and to date have mainly been based on hosts that have limited chemical and thermal stability. Here we identify Noria, a rigid cyclic oligomer as a new host for the synthesis of more robust Type II PLs. Although the structure of Noria is well-documented, we find that literature has overlooked the true composition of bulk Noria samples. We find that bulk samples typically consist of Noria (*ca.* 40%), a Noria isomer, specifically a resorcinarene trimer, "R3" (*ca.* 30%) and other unidentified oligomers (*ca.* 30%). Noria has been characterised crystallographically as a diethyl ether solvate and its ^{1}H NMR spectrum fully assigned for the first time. The previously postulated but unreported R3 has also been characterised crystallographically as a dimethyl sulfoxide solvate, which confirms its alternative connectivity to Noria. Noria and R3 have low solubility which precludes their use in Type II PLs, however, the partially ethylated derivative Noria-OEt dissolves in the size-excluded solvent 15-crown-5 to give a new Type II PL. This PL exhibits enhanced uptake of methane (CH_4) gas supporting the presence of empty pores in the liquid. Detailed molecular dynamics simulations support the existence of pores in the liquid and show that occupation of the pores by CH_4 is favoured. Overall, this work revises the general accepted composition of bulk Noria samples and shows that Noria derivatives are appropriate for the synthesis of more robust Type II PLs.

Received 21st June 2021
Accepted 10th October 2021

DOI: 10.1039/d1sc03367k

rsc.li/chemical-science

Introduction

Porosity is a useful fundamental characteristic of materials that has led to a variety of large-scale applications.[1,2] Conventionally, permanent porosity has only been associated with solid state materials. This is intuitively reasonable since the relatively static nature of solids at the molecular level can enable empty cavities to persist. Porosity in liquids has conventionally been limited to the small, transient and irregular voids that are generated between molecules of the liquid as they tumble.[3–5] However, strategies for generating large, permanent and well-defined pores in liquids have recently been proposed and demonstrated.[6,7] For example, if discrete host molecules with rigid structures can be dissolved in solvents which cannot enter the host's cavities, then the resulting solutions will have persistent empty pores. The resulting counter-intuitive materials are termed Porous Liquids (PLs), with those based on empty hosts dissolved in size-excluded solvents categorised as Type II PLs. The selection/design of appropriate hosts for generating Type II PLs is not trivial since several criteria must be satisfied.[6] Specifically, the host must, (i) be rigid (*i.e.*, not collapse in the absence of a guest) so that its cavity persists, (ii) sterically exclude the solvent used (which also makes the choice of solvent a critical part of the design of the PL), (iii) be highly soluble in the solvent used if useful bulk properties (*e.g.*, gas solubility) are to be maximised. To date, only a limited number of host types have been experimentally demonstrated for the formation of Type II PLs. They include *T*-symmetry iminospherand organic cages[7,8] tetrahedral Zn(II) coordination cages[9] and $Cu(II)_{24}$ 'nanoball' coordination cages (MOP-18).[10] Notably, such hosts all have limited chemical stability in solution (*e.g.*, to water, acids, and bases). This is in contrast to Type III PLs, *i.e.*, those composed of microporous solids dispersed in

[a]*School of Chemistry and Chemical Engineering, Queen's University Belfast, David Keir Building, Stranmillis Road, Belfast, BT7 1NN, UK. E-mail: s.james@qub.ac.uk*
[b]*ICB-CONICET, Facultad de Ciencias Exactas y Naturales, Universidad Nacional de Cuyo, Padre Jorge Contreras 1300, Mendoza, M5502 JMA, Argentina*
[c]*EPSRC National Crystallography Service, School of Chemistry, Faculty of Engineering and Physical Sciences, University of Southampton, Southampton, SO17 1BJ, UK*
[d]*School of Chemistry and Bioscience, University of Bradford, Richmond Road, Bradford, BD7 1DP, UK*

† Electronic supplementary information (ESI) available. CCDC 2080523 and 2080524. For ESI and crystallographic data in CIF or other electronic format see DOI: 10.1039/d1sc03367k

size-excluded liquids, which exhibit high chemical and thermal stability.[11–14] Therefore, developing Type II PLs that are more chemically robust as well as economical to prepare would be a significant step toward enabling applications for these materials. Chemically robust macrocyclic hosts such as calix[*n*]arenes,[15] cucurbiturils[16] and pillar[*n*]arenes[17] have been extensively investigated for various applications but not in the context of PLs. Drawbacks of these hosts in this regard variously include insufficient rigidity and/or solubility. However, further host molecules have been developed from calix[*n*]arenes such as cavitands, carcerands and more recently the paddle-wheel shaped host referred to as Noria.[18a] Noria does have potential for the synthesis of Type II PLs since in addition to having a significant central cavity (*ca.* 5 Å in diameter), it has an apparently rigid structure as well as 24 external hydroxyl groups which can be functionalised to provide high solubility. Also, it is reported to be easily prepared in one step from inexpensive starting materials (resorcinol and 1,5-pentanedial).[18a]

In this paper, we explore the use of Noria and its derivatives for the formation of Type II PLs. To this end, we have revisited its synthesis and characterisation, and have obtained detailed insight into the true composition of bulk samples of Noria (as obtained by the standard literature procedure) for the first time. In particular, material prepared by the standard literature method was found to consist of only *ca.* 40% Noria, with 30% being an additional high symmetry species identified as a resorcinarene trimer, "R3", which is an isomer of Noria and 30% other oligomers. Noria at higher purity (*ca.* 60%) has been obtained and its proton nuclear magnetic resonance (^{1}H NMR) spectrum fully assigned for the first time. The previously postulated but unreported isomer R3 has also been fully characterised including an X-ray crystal structure. We have also investigated the more soluble derivative, Noria-OEt, in which 12 ethyl substituents are scrambled over the 24 external O sites, for the synthesis of PLs.[19] Experimental gas uptake measurements and detailed molecular dynamics (MD) modelling suggest that Noria-OEt dissolved in 15-crown-5 is indeed a new chemically and thermally robust Type II PL.

Results and discussion

The structure of Noria and the composition of bulk Noria samples – previous work

Kudo *et al.* first synthesised Noria in 2006 by the acid-catalysed co-condensation of resorcinol and 1,5-pentanedial.[18a] They also reported two derivatives, Noria-BOC and Noria-COOEt, in which the 24 external –OH groups were functionalised with *tert*-butoxycarbonyl or ethoxycarbonyl groups, respectively.[18a] Through single crystal X-ray analysis of Noria-BOC, the core connectivity of the Noria host was established to have the S_6 symmetry topology depicted in Fig. 1.

In fact, Kudo *et al.* had expected to obtain an alternative structure, a resorcinarene trimer herein denoted "R3", which is a structural isomer of Noria (Fig. 1).[18a] Subsequently other analogous trimeric structures with methylene chains of different lengths (R–$(CH_2)_n$–R, n = 5, 7, 9)[18b] as well as dimeric structures with even-number methylene chains have been

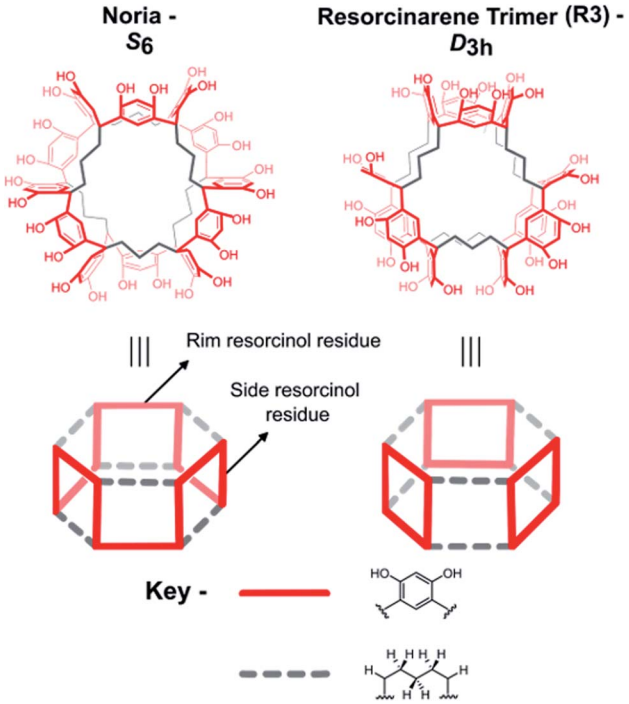

Fig. 1 Comparison of the structures of the isomeric Noria and resorcinarene trimer (R3).

reported in the literature.[18c–e] Although Noria and R3 have different topologies with regard to the positions of the resorcinol and 1,5-pentanedial residues, they each have high symmetry (S_6 and D_{3h} respectively) and remarkably similar overall structures in that each has shallow cavities around the periphery and a single larger 5 Å hydrophobic cavity at the centre. Further characterisation of Noria by Kudo *et al.* included ^{1}H NMR spectroscopy, infrared (IR) spectroscopy and mass spectrometry (MS).[18a] However, for the ^{1}H NMR spectrum only ranges of chemical shift rather than specific values were quoted for each chemically distinct proton. In 2010 the ^{1}H NMR spectrum itself was reported, which is reproduced with the assignment ranges indicated in Fig. 2a.[20]

The ^{1}H NMR spectrum shown in Fig. 2(a) is too broad and complex to be consistent with the crystallographically determined S_6 topology of Noria, which would have, for example, only two chemically distinct –OH groups, and four chemically distinct ArH protons due to the presence of only two chemically distinct ('rim' and 'side') aromatic rings. In the ^{1}H NMR spectrum, all proton environments manifest as broad features upon which several sharper peaks are superimposed. Computational prediction of the ^{1}H NMR spectra by Peerannawar and Gejji *et al.*[21] also supports the assertion that the ^{1}H NMR spectrum of Noria should be far simpler than observed. Further, in 2018, Zhai *et al.* reported a ^{1}H NMR spectrum (Fig. 2(b)) which is indeed simpler and consistent with the S_6 Noria structure.[22] For example, it shows the expected two –OH signals and four ArH signals, together with some impurities. However, this spectrum was not fully interpreted, especially regarding the methylene groups of the 1,5-pentanedial residues. Also, no purification

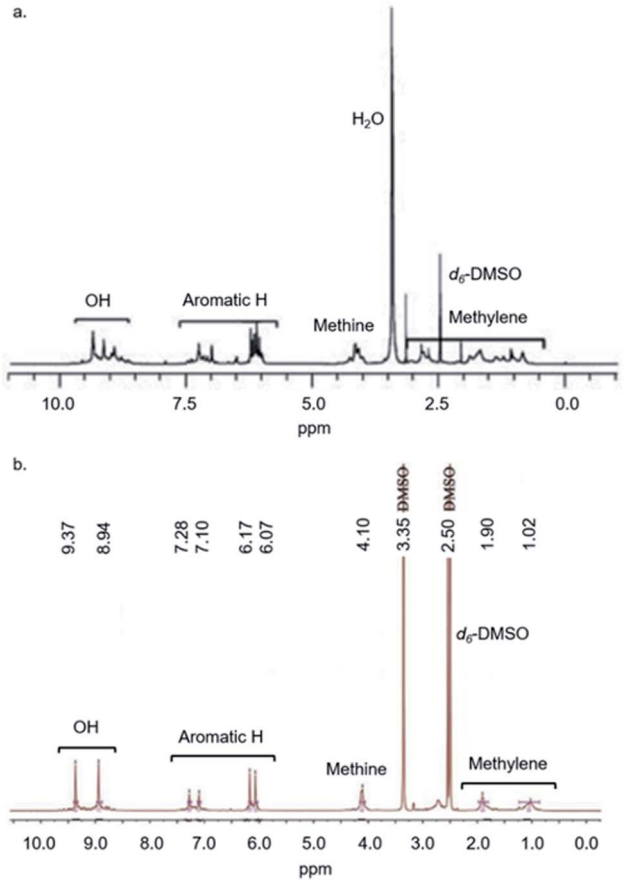

Fig. 2 (a) ^{1}H NMR spectrum of Noria reported by Kudo *et al.*, adapted from ref. 20. (b) ^{1}H NMR spectrum of Noria reported by Zhai *et al.*, adapted from ref. 22. Note the peak at 3.35 ppm may be due to water.

procedure was given, so it is not clear how an apparently purer bulk material was obtained than in the preceding reports. In 2009, Tian *et al.* determined the structure of Noria itself by single crystal X-ray diffraction[25] and found the same S_6 topology as in the crystal structure of Noria-BOC as determined by Kudo *et al.*[18a] Analysis by powder X-ray diffraction[25] has shown that bulk samples of Noria are amorphous. Derivatives of Noria in which the –OH protons are substituted with various R groups have also been reported.[23,24] In all cases found in the literature, ^{1}H NMR data for bulk samples of Noria derivatives have also exhibited broad signals that are not consistent with pure, high-symmetry products. Very recently, a ^{1}H NMR spectrum has been reported by Shimoyama *et al.*,[27] which is consistent with the S_6 symmetry, but with different chemical shifts to the ^{1}H NMR spectrum reported by Zhai *et al.* (see ESI, S2.14†).[22] Despite the overall lack of definitive characterisation of bulk Noria samples, in terms of the functional porosity of bulk Noria samples, gas sorption isotherms do point to significant microporosity consistent with the nature of Noria as a rigid host with a central cavity.[25,26]

Overall, the existing literature can be summarised as follows: (1) there is clear evidence for the generally accepted S_6 core connectivity of Noria (from X-ray crystal structures of Noria and Noria-BOC),[25,18a] (2) despite this, in all but two cases,[22,27] solution state ^{1}H NMR spectra of bulk Noria samples are inexplicably broad and contain too many peaks than can be accounted for by this S_6 topology structure, (3) the two better-resolved ^{1}H NMR spectra reported by Zhai *et al.* and Shimoyama *et al.* differ to each other in terms of chemical shifts suggesting that they were observing different species.[22,27] This points to bulk samples of Noria and its derivatives having greater structural/compositional complexity than is apparent from the two crystal structure determinations and which is generally recognised in the literature *i.e.*, bulk samples of Noria seem to be crude.

Revision of the composition of Noria bulk samples – this work

In this work, our aim was to develop Type II PLs based on Noria. We therefore began by re-synthesising Noria according to the original literature method described by Kudo *et al.* and obtained bulk samples with ^{1}H NMR spectra similar to the broad and complex ones reported in the literature which are not consistent with a pure S_6 Noria structure.[18a,20] As previously mentioned, a recent paper published by Shimoyama *et al.*[27] stated that bulk Noria samples were comprised of a mixture of species, however, no detail was given as to what these species were, other than that they may be polymeric byproducts. The lack of consistency regarding the ^{1}H NMR spectrum of Noria found in the literature was concerning and necessitated systematic studies into the true nature of bulk Noria samples. Variable temperature ^{1}H NMR experiments were firstly conducted to probe the possibility of dynamic behaviour (see ESI Fig. S30†). However, the spectra did not change significantly between 25 and 120 °C (in deuterated dimethyl sulfoxide (d_6-DMSO)). Therefore, the complexity and broadness were concluded to indicate that a mixture of species was indeed present, in agreement with Shimoyama *et al.*[27] Liquid chromatography-mass spectrometry (LCMS) analysis was inconclusive on this point because of low solubility in appropriate solvents such as acetonitrile, and we therefore investigated various bulk separation and purification procedures to elucidate the composition (Fig. 3).

These procedures generated six solid samples (Products 1–7) as follows:

Product 1: (crude Noria) Noria was synthesised according to the literature procedure of Kudo *et al.*[18a] and was obtained as a yellow powder. As stated above, ^{1}H NMR spectra were broad and contained too many signals (see below), similar to the spectrum reported by Kudo *et al.*[18a,20]

Product 2: (recrystallised material) Product 1 was recrystallised from DMSO and MeOH (process 2 in Fig. 3) to give a cream-coloured powder. This procedure was used because Noria single crystals were reportedly grown from DMSO/MeOH.[25] Also, in the ^{1}H NMR spectrum of the apparently purer material reported by Zhai *et al.*[22] (Fig. 2(b)) a peak due to H_6-DMSO is present in addition to residual D/H-DMSO (d_6-DMSO was used as the ^{1}H NMR solvent) suggesting that the purification procedure they used involved DMSO. The ^{1}H NMR spectrum of Product 2 (see Fig. 4) did indeed match well with that reported by Zhai *et al.*[22] with all major peaks matching in terms

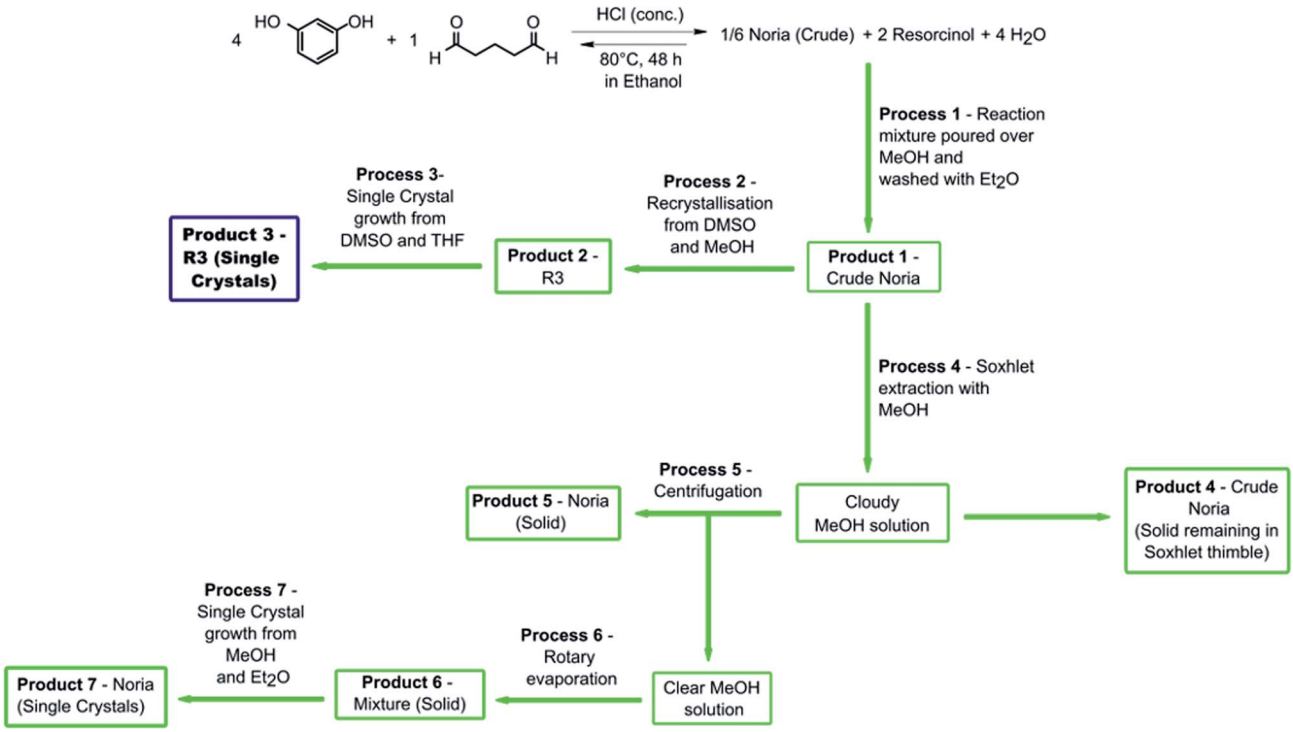

Fig. 3 A flowchart showing the procedures applied and products obtained in the purification of crude Noria. Note that the blue box highlights R3, a previously unreported cyclic molecular host and structural isomer of Noria. Further details can be found in the ESI.†

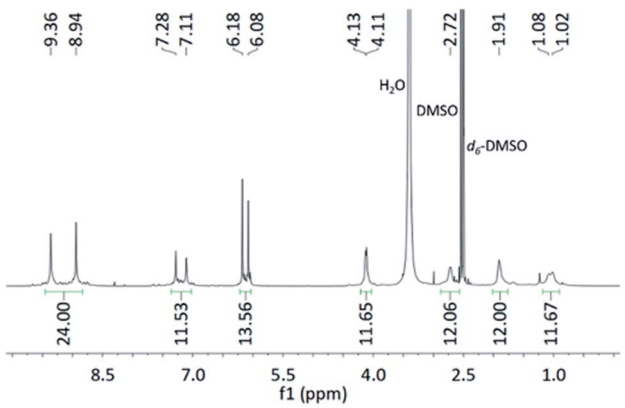

Fig. 4 ^{1}H NMR spectrum of the recrystallised material, Product 2.

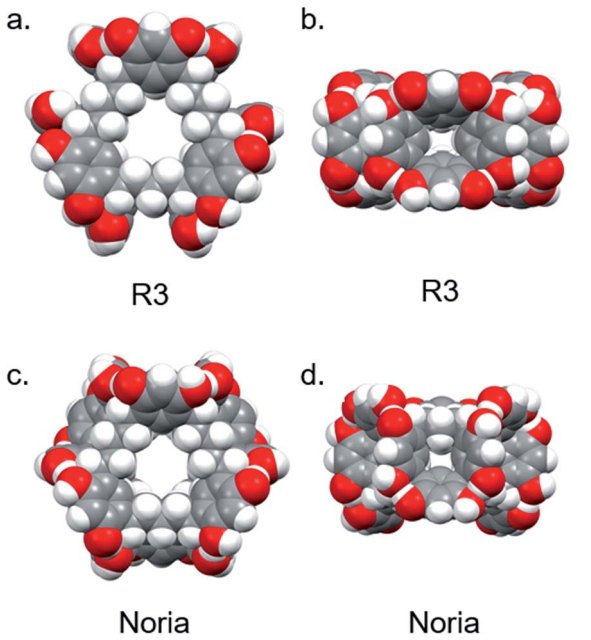

Fig. 5 X-ray crystal structures of R3 (Product 3) and Noria (Product 7). (a) R3 'top view' showing the central cavity and the three resorcinarene units on the exterior, (b) R3 'side view' showing one of the resorcinarene units defined by four neighbouring aryl groups, (c) Noria 'top view' showing the central cavity; (d) Noria 'side view' showing the 'sinusoidal' chain of aryl groups. All solvent molecules have been omitted for clarity.

of chemical shift, multiplicity, and integration. There are some impurities present according to the ^{1}H NMR spectrum, and we thus estimate (by peak integration) the level of purity of Product 2 to be >70%.

Product 3: (single crystals of R3) Product 2 was washed with dimethylformamide (DMF) and the residue crystallised over several weeks by vapour diffusion of tetrahydrofuran (THF) into a DMSO solution to give colourless plate-like single crystals suitable for X-ray analysis (Product 3). Interestingly, the structure was determined not to be that of Noria but instead R3 (Fig. 5(a) and (b)).

Product 3 crystallises as a DMSO solvate in the triclinic space group $P\bar{1}$. Although there are several solvent molecules present

in the structure some were too disordered to be suitably modelled and therefore solvent masking was employed. Notable features of the R3 molecules are the resorcinarene trimer connectivity with idealised D_{3h} symmetry. In contrast to the sinusoidal chain of aryl rings in Noria the aryl rings in R3 are arranged into three resorcinol tetramers such that three large, well-defined concavities exist on the outside surface (Fig. 5(a)), each occupied by a single DMSO molecule. There is a central cavity which can accommodate a sphere of diameter 4.88 Å as inferred from the distance from molecular centroid to the nearest H atom, taking into account the van der Waals radius. This cavity is also occupied by DMSO and is very similar in size and shape to the cavity of Noria (see below).There is extensive intramolecular hydrogen bonding between the hydroxyl groups of neighbouring aryl rings, as well as intermolecular hydrogen bonding between R3 molecules such that they form dimers within the crystal (Fig. S48†). The dimers are interspersed by further solvent molecules to form columns. These columns pack in a hexagonal arrangement with additional solvent molecules between them (Fig. S48†). Within the R3 molecules all bond lengths and angles are unremarkable. Some of the single crystals of R3 were dissolved in d_6-DMSO and ^{1}H NMR spectroscopy confirmed that it matched the material from which it was crystallised (Product 2) confirming that Product 2 is definitively R3. The purity was higher than Product 2 and estimated to be *ca.* 90% (see ESI Section S2.3†). Therefore, the ^{1}H NMR spectrum in the report of Zhai *et al.*[22] relates to R3 rather than Noria. The ^{1}H NMR spectrum of Product 2 is fully consistent with the crystallographically-determined D_{3h} symmetry of R3 (for example there are two –OH signals and four aromatic (ArH) signals, corresponding to the two chemically distinct resorcinol residues (refer to Fig. 4). Further, we have fully assigned all peaks in the spectrum including the more complex region due to the methylene protons of the 1,5-pentanedial residues for the first time. In particular, the signal at 2.72 ppm, which was previously not assigned as a product peak,[22] was in fact shown by 2D NMR experiments to belong to the C_5 chain (see ESI Section S2.2, Fig. S5–S10†). Four resonances in the alkyl region can be fully accounted for by the expected inequivalence of mutually geminal protons in CH_2 groups in the C_5 chain. In particular, the central CH_2 group resonates at 1.02 and 1.08 ppm and its neighbouring CH_2 units at 1.91 and 2.72 ppm (the methylene protons were assigned on the basis of the angular dependence of vicinal coupling constants). The CH methine resonance appears at 4.12 ppm. The matrix-assisted laser desorption/ionization time-of-flight (MALDI-TOF) mass spectrum was also consistent with the structure of R3, showing clear peaks for the ions $[M + Na]^+$, $[M + Na + DCTB]^+$ and $[M + Na + 2DCTB]^+$ (DCTB = *trans*-2-[3-(4-*tert*-butylphenyl)-2-methyl-2-propenylidene]malononitrile matrix) (see ESI Fig. S11 and S12†).

The above crystallographic and NMR spectrometric analysis not only suggests that previous literature in which the same ^{1}H NMR data was assigned to the S_6 Noria structure (with which it is also consistent) should be reconsidered,[22] but also reveals that the crude Noria material as reported in the literature more generally actually consists substantially (*ca.* 30%) of the isomeric structure R3 (see further discussion below).

Soxhlet extraction of Product 1 with MeOH was also investigated as an alternative purification method. This generated four additional samples, Products 4–7:

Product 4: solid remaining in the Soxhlet thimble.

Product 5: a precipitate in the MeOH extract that was collected by centrifugation.

Product 6: material dissolved in the MeOH extract supernatant that was isolated by evaporation of the solvent.

Product 7: single crystals grown from Product 6 by vapour diffusion of Et_2O into a MeOH solution.

Products 4–7 were analysed by ^{1}H NMR spectroscopy (see ESI Sections S2.4, S2.5, S2.6 and S2.7†).

Products 4 and 6 were both found to be similar in composition to Product 1 (*i.e.*, crude Noria) as indicated by their similar ^{1}H NMR spectra.

Since Product 6 had high solubility in MeOH, and Noria is reported to have low solubility in MeOH,[20] we attempted to grow single crystals of this apparently unknown material by vapour diffusion of Et_2O into a MeOH solution in the expectation of obtaining a new, non-Noria species. Single crystals (Product 7) were obtained over the course of several weeks but surprisingly, the X-ray structure determination revealed that Product 7 was Noria (Fig. 5(c) and (d), ESI Section S2.7†), obtained as a MeOH–Et_2O solvate. The same overall topology with S_6 symmetry is observed as in the previous structure determinations of Noria and Noria-BOC mentioned above. Within the structure all bond lengths and angles are unremarkable, and the central cavity can accommodate a sphere of diameter 4.98 Å as inferred from the distance from molecular centroid to the nearest H atom, taking into account the van der Waals radius. Thus, the cavities of the Noria and R3 are very similar in size. The cavity contains disordered MeOH molecules. There are additional interstitial solvent molecules, specifically one MeOH molecule which donates a hydrogen bond to an Ar–OH group of the Noria and one Et_2O molecule which occupies one of the shallow external

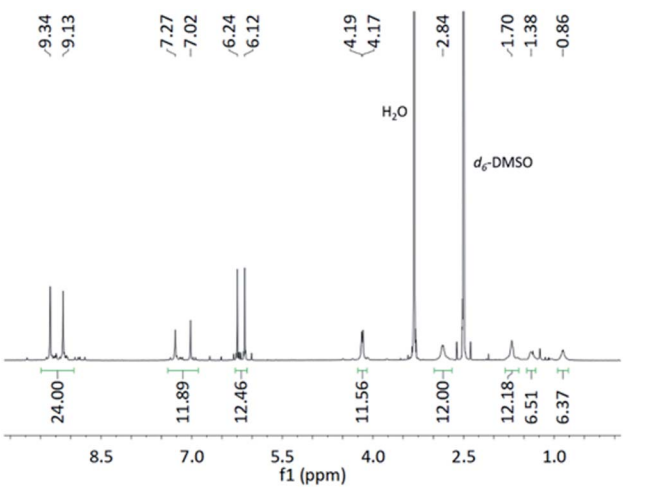

Fig. 6 ^{1}H NMR Spectrum of Product 7 which was obtained as single crystals.

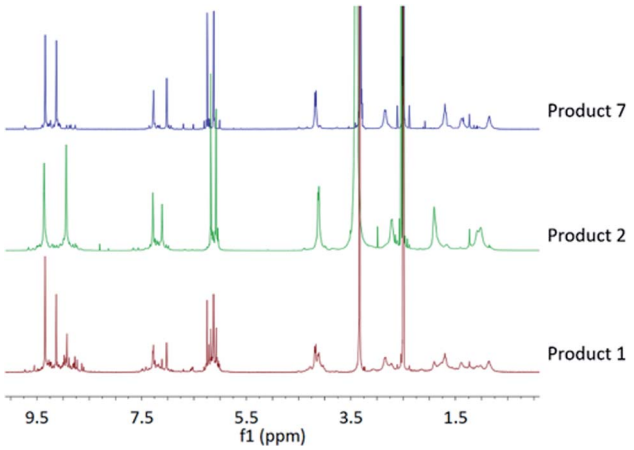

Fig. 7 Overlay of ^{1}H NMR spectra for Product 1, 2 and 7, showing that both Noria and R3 are present in the crude Product 1.

cavities. The Noria molecules are arranged in columns along the *c* axis which pack hexagonally (Fig. S47†). The ^{1}H NMR spectrum of Product 7 was obtained by dissolving some single crystals in d_6-DMSO and it was found to match well with the spectrum reported by Shimoyama *et al.*[27] However, we have also now fully assigned the spectrum (see ESI Section S2.5 and S2.7†). (Fig. 6) and it should be noted that it was found to match very closely to that Product 5 in terms of chemical shifts, multiplicities, and integrations (see ESI Section S2.5†).

Although perhaps unlikely, we considered the possibility that some interconversion between Noria and R3 isomers might occur (*i.e.*, do they form simultaneously during synthesis, or do they interconvert during the work-up?). Inspection of the ^{1}H NMR spectrum of Product 1 reveals that both species are in fact present in the crude material (Fig. 7), suggesting that both species form during the synthesis itself.

From the ^{1}H NMR spectrum of Product 1 (crude Noria) it is also clear that other species in addition to Noria and R3 are present. We suggest that these are further linear and/or cyclic oligomers. From the ^{1}H NMR spectrum we estimate the relative amounts of the various species present to be 40% Noria, 30% R3 and 30% other oligomers.

In summary, the above analysis suggests the following key points:

(1) Bulk samples of Noria as obtained by the standard literature procedure, are actually crude and consist of a mixture of Noria, R3 and other oligomers.

(2) Samples consisting primarily of R3 can be obtained by recrystallisation of Product 1 from DMSO/MeOH.

(3) Single crystals of R3 can then be obtained by crystallisation from DMSO/THF.

(4) Samples consisting primarily of Noria can be obtained from Product 1 by Soxhlet extraction with MeOH.

(5) Noria single crystals can then be obtained by crystallisation using MeOH/Et_2O.

Given the above revision of the composition of bulk Noria samples (crude), it is important to consider any implications for the previously observed properties of this bulk crude material in the literature. Firstly, the reported amorphous nature of the material[25] is fully consistent with a mixture of isomeric and oligomeric species being present. Secondly, the ability of the bulk crude material to adsorb gases in the solid state[25,26] (*i.e.*, to exhibit microporosity) is still consistent with the revised composition since the bulk crude material consists around 70% of rigid hosts with cavities (albeit a combination of Noria and R3, rather than pure Noria) which according to X-ray analysis are likely to have similar host properties to each other. It is also conceivable that larger cyclic oligomers may be present which could also exhibit porosity. We note that there have been no detailed studies of guest inclusion with Noria in solution to date. We suggest that such studies may not have been feasible because of the ill-defined ^{1}H NMR spectra and lack of understanding of the true composition of bulk samples. Finally, we note that the solubilities of Noria and R3 samples unsurprisingly seem to be affected by their levels of purity, with solubility generally decreasing markedly as purity increases. This variable solubility may also have hampered attempts to understand and elucidate the composition of bulk samples.

Noria as a host for Type II PLs

As noted in the introduction, for a host to be appropriate for forming Type II PLs it should be unable to collapse when empty and soluble in a size-excluded solvent. The Noria structure appears to satisfy the first criterion according to MD modelling as discussed below. Also, it shows excellent stability which is important if Type II PLs are to be considered at some point for applications. For example, it is soluble in alkaline water (pH 10) and ^{1}H NMR spectra showed it to be unchanged after 5 days. Also, heating to 100 °C for 7 days in wet d_6-DMSO showed no significant changes in ^{1}H NMR spectra (see ESI S2.11 and S2.12†). However, it has low solubility in all solvents investigated and we therefore turned attention to the known semi-ethylated derivative Noria-OEt.[19]

Synthesis and characterisation of Noria-OEt and formation of a Type II PL in 15-crown-5

Noria-OEt, has been synthesised previously by co-condensation of 3-ethoxyphenol and 1,5-pentanedial under acidic conditions.[19] The 12 ethyl groups of Noria-OEt are expected to be scrambled over the 24 external O sites of the S_6 core structure. Hence, bulk Noria-OEt is likely to exist as a complex mixture of up to 64 geometrical isomers (see ESI Fig. S36†). Although this complicates the analysis of the material, such scrambling of substituents can be an advantage in that it can lead to higher solubility.[7] We repeated the published synthesis with some slight adaptations (see ESI Section S2.13†).[19] Evidence for the expected product was seen in the MALDI-MS spectrum which showed expected peaks for $[M]^{+\bullet}$, $[M + Na]^+$, $[M + K]^+$ as well as inclusion complexes with the DCTB matrix (see ESI Section S2.13.1, Fig. S34†). Due to the scrambling of the ethyl groups, however, the ^{1}H NMR spectrum of Noria-OEt is expected to be complex. This was indeed the case with each chemically distinct proton environment showing as a broad feature (see ESI Section S2.13, Fig. S33†). Despite this, the relative integrations of these

features matched with the expected overall structure, the spectrum closely matched that in the literature[19a] and there were no peaks which would suggest that other types of product might be present. It is important to consider that Noria-OEt may also contain the R3-OEt structure and other oligomers analogous to those seen in bulk samples of Noria itself. However, because of the inherent complexity of the ^{1}H NMR spectrum due to the scrambling, it was not possible to draw firm conclusions on this from the ^{1}H NMR spectrum alone. Further, attempts at LCMS analysis were not successful because of its low solubility in appropriate solvents such as acetonitrile. However, as noted above, both the D_{3h} (R3) and S_6 (Noria) topologies possess central cavities of similar size (see also below). Thus, if Noria-OEt were to consist of both R3-OEt and Noria-OEt, then both hosts should give rise to pores in the liquid state when dissolved in a size-excluded solvent. It was found that Noria-OEt had significant solubility (up to 80 mg mL^{-1}) in the bulky solvent 15-crown-5. The bulky solvent 15-crown-5 has a diameter of approximately 10 Å (measured between the most distant H atoms including van der Waals radii) and a low surface curvature, which has enabled it to be used successfully as a size-excluded solvent in PLs based on imino-spherand cages and coordination cages.[7,10] Consequently, it seemed likely that such 15-crown-5 solutions of Noria-OEt would constitute new Type II PLs. MD modelling and gas solubility measurements were performed to substantiate the presence of permanent pores in such solutions and to investigate more generally the structure of this putative PL phase.

Molecular dynamics modelling of Noria-OEt-15-crown-5 PL

MD simulations were performed at 300 and 350 K, both at 1 atm. The liquid consisted of Noria-OEt dissolved in 15-crown-5 at a 1 : 206 molar ratio, which corresponds to the 50 mg mL^{-1} concentration used in the gas solubility measurements described below (see Fig. 14). As a reference, simulations of the neat solvent were conducted at the same temperatures and pressure. Atomistic models for the Noria-OEt host and the solvent were constructed from the Optimised Potentials for Liquid Simulations (OPLS) all-atom force-field, with atomic charges obtained from *ab initio* Density Functional Theory (DFT) methods and equilibrium reference geometries. For simplicity, a single Noria-OEt isomer was modelled, with –OH and –OEt groups arranged in an alternating fashion on the outside of the molecule so that the OEt groups were maximally spaced. Further information on model parameters, simulation details and electronic structure calculations is provided in the ESI (S5).† As expected, throughout the MD simulation runs, 15-crown-5 solvent molecules were unable to occupy the central Noria-OEt cavity due to steric hindrance. This exclusion is reflected in the large formation energy of the Noria-OEt solvent inclusion complex, estimated with DFT methods as +90.96 kcal mol^{-1}. Moreover, no minimum was observed below 0.6 nm in the free energy landscape of the inclusion complex, calculated by MD-based umbrella sampling simulations using the distance ξ between the centres of mass of the host and the solvent molecule as reaction coordinate (Fig. 8). The free energy

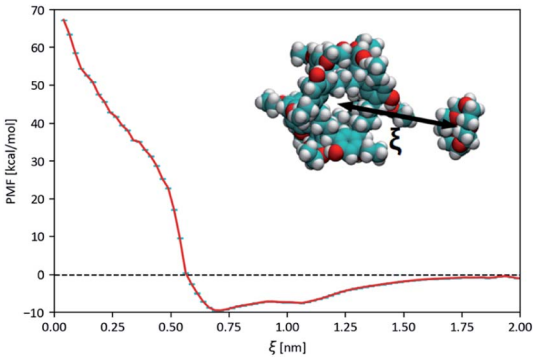

Fig. 8 Potential of Mean Force (PMF) computed by umbrella sampling for the inclusion of a 15-crown-5 molecule in a Noria-OEt host in vacuum at 350 K. As illustrated in the inset, the reaction coordinate ξ corresponds to the distance between their centres of mass. Error bars are shown in light blue.

curve features a global minimum at 0.71 nm, *i.e.*, with 15-crown-5 sitting outside the cavity entrance and rises sharply as the solvent molecule enters the cavity. The maximum corresponds to a 67.28 kcal mol^{-1} energy difference relative to the average asymptotic value.

Furthermore, the host–solvent radial distribution function, $g(r)$, for the 1 : 206 Noria-OEt–solvent system illustrates that solvent molecules remained outside the central cavities during the 100 ns simulations, with unbiased MD trajectories (Fig. 9).

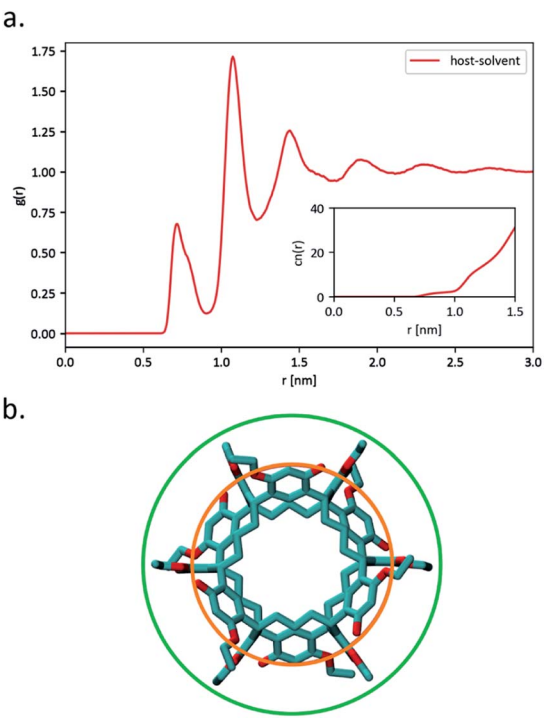

Fig. 9 (a) Radial distribution function, $g(r)$, between the molecular centres of Noria-OEt hosts and 15-crown-5 molecules in a 1 : 206 mixture at 350 K and 1 atm. The inset shows running coordination numbers, cn(r). (b) Locations of the first (orange) and second (green) maxima of the host–solvent $g(r)$ from a top perspective of the Noria-OEt host.

Further analysis of the host–solvent radial distribution function (Fig. 9(a)) shows two distinct solvation shells at 0.72 nm and 1.08 nm. These values highlight two structural features of interest illustrated in Fig. 9(b): the distance between the centre of the host and the solvent molecules located at any of the six lateral indentations outside Noria-OEt (orange circle), and the outer effective radius of the host as outlined by the solvent (green circle). In addition to their structural significance, both distances correspond to the minima in the PMF curve of the inclusion complex (Fig. 8). The minimum at 0.72 nm also hints that the shallow outer indentations of the Noria-OEt host accommodate some solvent molecules (~2 on average) in the liquid phase, unlike the inner intrinsic cavity. Since solvent molecules remain outside the intrinsic cavity of a Noria-OEt host, dissolving Noria-OEt in 15-crown-5 is expected to introduce additional empty cavities in this solvent. To quantify this effect, we calculated the insertion probability $P(R)$, which represents the likelihood of being able to insert a hard sphere of radius R at a random point in the liquid.[28] Furthermore, we previously defined the relative porosity $W(R)$ as the quotient between $P(R)$ in the PL and in the neat solvent (at the same temperature and pressure).[7] We calculated $P(R)$ from MD simulations of both liquids at 300 and 350 K. 1000 configurations were selected and probed every 0.05 nm along the x, y and z axes to find the largest sphere that could be inserted without overlapping the van der Waals radius of any atom. The resulting $W(R)$ curves are shown in Fig. 10.

$W(R) > 1$ indicates that for a probe radius R, the concentration of cavities in the PL is greater than in the neat solvent. While both curves feature a maximum at approximately 0.20 nm, the increase of porosity at 300 K is much steeper. Relative to the neat solvent, the PL has seven times more cavities whose radii are roughly 0.20 nm. At 350 K, however, this relative factor is approximately 1.54. This contrast suggests that the increase in porosity in the PL stems primarily from the presence of intrinsic Noria-OEt cavities: a fixed number of intrinsic cavities has a greater effect on porosity when fewer (extrinsic) gaps exist between the solvent molecules, gaps that are more prevalent as temperature rises. Also, the peak in relative porosity occurs at the lower end of the average intrinsic cavity radius, estimated from simulations as 0.22 ± 0.02 nm, which reinforces the previous assessment. In order to assess how cavities are distributed in the space around the hosts, we calculated the radial distribution function of large cavities relative to the geometrical centre of the Noria-OEt molecules, $g_{cav}(r)$ (Fig. 11).

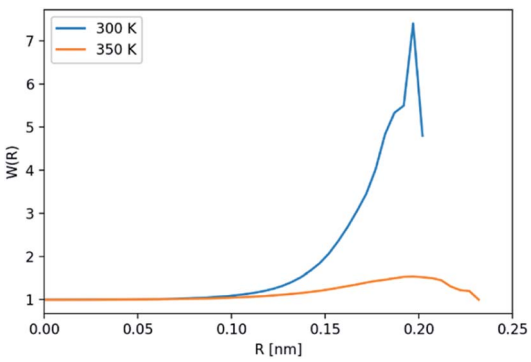

Fig. 10 Relative porosity, $W(R)$, of the PL obtained from MD simulations at 300 and 350 K. $W(R) = P^{PL}(R)/P^{Solv}(R)$, where $P^{PL}(R)$ is the insertion probability for spherical probe of radius R (ref. 28) in the PL, and $P^{Solv}(R)$ the corresponding insertion probability in the neat solvent at the same temperature.

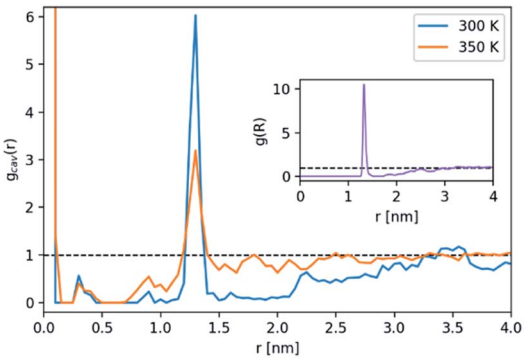

Fig. 11 Radial distribution function of large spherical cavities relative to the centres of hosts, $g_{cav}(r)$ for the simulated PLs at 300 and 350 K. The cavities considered had radii equal to or greater than 0.20 nm. Inset: host–host $g(r)$ for the 350 K liquid, featuring at ~1.3 nm a peak that matches the host-cavity radial distribution function.

This analysis comprised 100 configurations of each of the 300 and 350 K MD simulations of the PL and was restricted to cavities whose radii were equal to or greater than 0.20 nm. As expected, the large peaks in $g_{cav}(r)$ for $r \rightarrow 0$ nm stem from the fact that the host intrinsic cavity is empty. Outside the hosts, however, a large maximum was found at ~1.3 nm for both temperatures. As evidenced by the host–host $g(r)$ included as an inset in Fig. 11, this peak arises from Noria-OEt dimers that remained stable throughout the simulations. Other than this maximum, no discernible trends in cavity distribution were observed beyond the effective radius of the hosts. In particular, there are no large cavities localised in the outer indentations of Noria-OEt. Fig. 12(a) and (b) illustrate the distribution of cavities in configurations selected from simulations at 300 and 350 K. Red and green surfaces indicate empty cavities inside or outside the hosts, respectively.

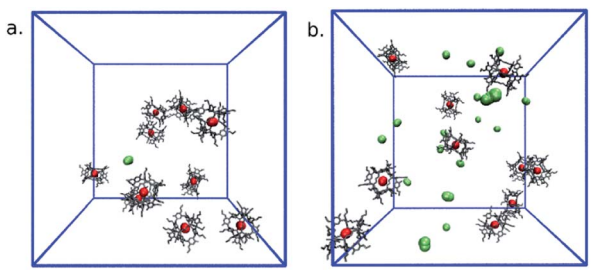

Fig. 12 Spatial distribution of intrinsic (red surfaces) and extrinsic cavities (green surfaces) in representative configurations of the PL at (a) 300 and (b) 350 K. To highlight the hosts, crown-ether solvent molecules have been omitted.

Overall, clearly the MD simulations reveal relevant details of the liquid structure, a key aspect being that 15-crown-5 is an appropriate size-excluded solvent for the formation a Type II PL based on Noria-OEt.

Methane solubility measurements

The existence of empty pores in PLs can lead to increased gas solubility as shown previously for Type II PLs based on other hosts.[7,8,10] For the methane (CH_4) solubility experiments with the suspected Noria-OEt PL, a high-pressure gas rig with gas flow monitoring was used as described elsewhere.[14] Solubilities were measured at 1, 2, 3, 4 and 5 bar at 303.15 K. Gas flow data confirmed that the system reached equilibrium well within the 1 hour period allowed for equilibration at each pressure. Data from three runs were averaged and compared with those for pure 15-crown-5 as a control (Fig. 13).

The presence of Noria-OEt clearly increases the CH_4 solubility, *e.g.*, at 1 bar from 0.13 mg g^{-1} for 15-crown-5 to 0.21 mg g^{-1} for the Noria-OEt PL. Although modest in comparison to more concentrated Type II PLs,[7] this increase is consistent with the lower concentration of the host species in this case. The excess solubility corresponds to *ca.* 0.22 CH_4 molecules per intrinsic cavity at 1 bar (see Fig. 14), which is an intuitively reasonable level of occupancy. As the pressure increases, the gas solubility remains consistently greater in the PL and reaches *ca.* 0.77 CH_4 molecules per cavity at 5 bar.

As a further control experiment, CH_4 solubility in a solution of 3-ethoxyphenol in 15-crown-5 was measured under similar conditions to check for the possibility that the increase in CH_4 solubility may be due to the presence of aromatic groups rather than actual intrinsic cavities. As shown in Fig. S41 in the ESI,† no increase in CH_4 solubility was observed, supporting the existence of cavities as being critical. Overall, the results from the gas uptake studies show that a solution of Noria-OEt in 15-crown-5, at a concentration of 50 mg mL^{-1}, does indeed exhibit an increase in CH_4 uptake compared to the solvent alone, and that the increase is in line with the expected level of porosity. Therefore, these measurements provide experimental evidence that this solution is a new Type II PL.

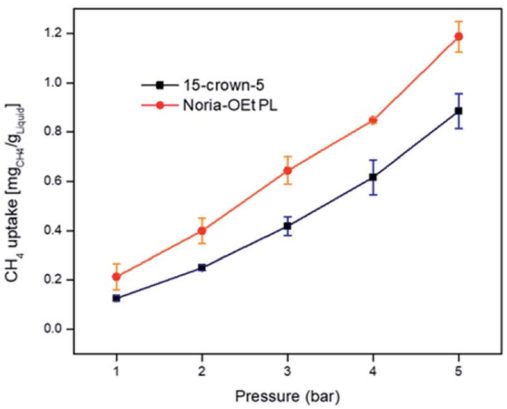

Fig. 13 CH_4 uptake at 303.15 K for 15-crown-5 average compared to Noria-OEt in 15-crown-5 (50 mg mL^{-1}) average (1–5 bar).

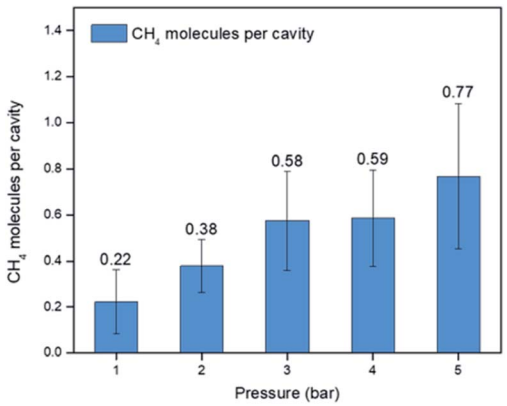

Fig. 14 Average number of CH_4 molecules per Noria-OEt cavity.

MD modelling of the PL with dissolved CH_4

To characterise the affinity of CH_4 for the Noria-OEt host, DFT-based geometry optimisation methods were used to calculate the formation energy of the host–CH_4 complex in vacuum. This complex was stable, with a favourable formation energy of −7.05 kcal mol^{-1}. In addition, the process of insertion of CH_4 into a host both in solution and vacuum was analysed through MD simulations and umbrella sampling. Fig. 15 shows the resulting free energy profiles at 350 K and 1 atm for the inclusion of a CH_4 molecule inside a single Noria-OEt molecule. For the system in solution, 341 15-crown-5 molecules were used.

The reaction coordinate, ξ, was defined as the distance between the host–guest centres of mass. In both landscapes, global minima occur at the centre of each intrinsic cavity and illustrate a strong tendency to form inclusion complexes of Noria-OEt and CH_4. Small minima are also observed at 0.8 nm, a distance that matches the valley between the first two peaks of the host–solvent $g(r)$ in Fig. 9(a). The inclusion of CH_4 into the Noria-OEt cage was more favourable in the liquid phase, *i.e.*, when the solvent was present, than in vacuum, suggesting that 15-crown-5 pushes the gas into the cages. This is further

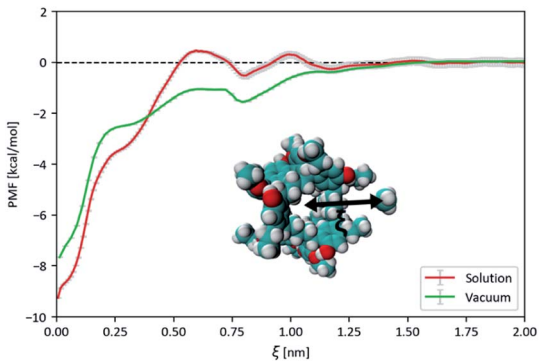

Fig. 15 Potential of Mean Force (PMF) computed by umbrella sampling for the inclusion of a CH_4 molecule in a Noria-OEt host in solution and vacuum at 350 K and 1 atm. The reaction coordinate ξ corresponds to the distance between their centres of mass. The dotted black line represents the average energy for ξ > 1.5 nm. Error bars are shown in grey.

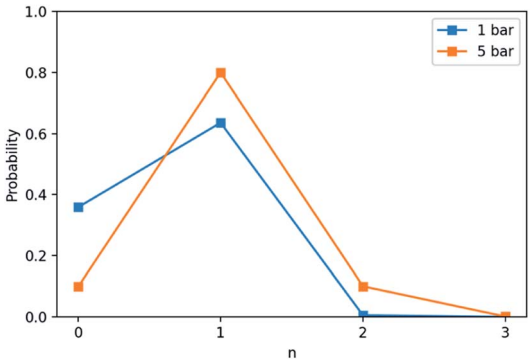

Fig. 16 Probability of finding n CH_4 molecules within 0.61 nm of Noria-OEt hosts in MD simulations of PLs at 350 K. The total amount of CH_4 was set in accordance with the experimental solubilities at 1 bar (blue) and 5 bar (orange).

confirmed by Fig. S44,† which shows the free energy profile for inserting a single CH_4 molecule inside a 15-crown-5 liquid slab, starting from vacuum. The resulting solvation free energy of CH_4 in the pure solvent at 350 K was 1.17 kcal mol^{-1}.

Further MD simulations were conducted on two PLs loaded with CH_4 and run at 350 K and either 1 or 5bar. Each system comprised 10 Noria-OEt hosts dissolved in 2060 15-crown-5 molecules, and the amount of CH_4 was set to correspond approximately to the experimental solubilities at each pressure: 7 gas molecules for the system at 1 bar pressure, and 36 molecules for the liquid at 5 bar. During the simulations, CH_4 remained predominantly inside the Noria-OEt intrinsic cavities. This is illustrated by the occupation probabilities, $p(n)$, shown in Fig. 16, where n represents the number of CH_4 molecules within 0.61 nm of the centre of mass of a host.

At 1 bar, hosts were 64% likely to be occupied, slightly below the maximum of 70% set by the 0.7 CH_4/Noria-OEt ratio. At 5 bar, occupation was 90% likely. Interestingly, at this higher pressure there was also 10% probability of double occupation, *i.e.*, of two CH_4 molecules being included in a single Noria-OEt cavity. The affinity of CH_4 to the Noria-OEt hosts is also reflected in large occupancy times, defined as the average span of time that a Noria-OEt hosts at least one CH_4 molecule without intermission. These values were 32.1 and 32.2 ns for the simulations at 1 and 5 bar, respectively.

Conclusions

In conclusion we have shown that Noria derivatives can be used for the synthesis of Type II PLs. As part of this work, we have substantially elucidated the composition of bulk (now known to be crude) Noria samples and revised the understanding in the literature. In particular rather than being a pure material, bulk samples of Noria prepared by the standard method consist of *ca.* 40% Noria, 30% R3 and 30% other oligomers. The partially ethylated derivative Noria-OEt dissolves readily in the size-excluded solvent 15-crown-5 to give a new Type II PL as supported by MD simulations and CH_4 solubility measurements. Such phases have the attraction of being inherently more chemically and thermally robust than Type II PLs reported to date and can also be synthesised economically. As such this represents a step toward Type II PLs which are more practical and may ultimately find applications. It also opens a new line of investigation for Type II PLs, specifically, other structures related to those here (*e.g.*, other oligomers, alternative peripheral functionalisation *etc.*) could be developed to provide a new family of Type II PLs which may accelerate the development of the field.

Data availability

Experimental, computational, and crystallographic data are provided in the ESI.†

Author contributions

FMA conducted the synthetic and analytical work. Gas solubility measurements were done by FMA. DEC contributed substantially to the technical analysis and interpretation. SLJ supervised the project. BPH contributed to ideation. MGdP, SFF and JLB conducted the MD simulation. PNH and SJC conducted the single crystal structure determination. The paper was drafted jointly by FMA, SLJ, MGdP, SFF and JLB. All authors have given approval to the final version of the manuscript.

Conflicts of interest

There are no conflicts to declare.

Acknowledgements

We acknowledge the National Mass Spectrometry Facility (NMSF) at Swansea University and in particular the useful discussions had with Dr Ann P. Hunter and Dr Mark F. Wyatt. MGDP acknowledges financial support from SECTyP-UNCUYO, ANPCyT (PICT-2015-1835), and SNCAD for computer time in the clusters Mendieta (CCAD-UNC) and Toko (UNCUYO). We also acknowledge funding from EPSRC, grant number: EP/R005540/1.

Notes and references

1 P. A. Wright, Chapter 1 Introduction, in *Microporous Framework Solids*, The Royal Society of Chemistry, 2008, pp. 1–7.
2 F. Romm, *Microporous Media*, Marcel Dekker, New York, 2004.
3 A. Pohorille and L. R. Pratt, *J. Am. Chem. Soc.*, 1990, **112**, 5066–5074.
4 G. Graziano, *Biophys. Chem.*, 2003, **104**, 393–405.
5 S. Sastry, T. M. Truskett, P. G. Debenedetti, S. Torquato and F. H. Stillinger, *Mol. Phys.*, 1998, **95**, 289–297.
6 (*a*) N. O'Reilly, N. Giri and S. L. James, *Chem.–Eur. J.*, 2007, **13**, 3020–3025; (*b*) S. L. James and B. Hutchings, in *Funct. Org. Liq.*, ed. T. Nakanishi, Wiley-VCH, 2019, pp. 39–52.

7 N. Giri, M. G. Del Pópolo, G. Melaugh, R. L. Greenaway, K. Rätzke, T. Koschine, L. Pison, M. F. C. Gomes, A. I. Cooper and S. L. James, *Nature*, 2015, **527**, 216–220.
8 K. Jie, N. Onishi, J. A. Schott, I. Popovs, D. Jiang, S. Mahurin and S. Dai, *Angew. Chem., Int. Ed.*, 2020, **59**, 2268–2272.
9 L. Ma, C. J. E. Haynes, A. B. Grommet, A. Walczak, C. C. Parkins, C. M. Doherty, L. Longley, A. Tron, A. R. Stefankiewicz, T. D. Bennett and J. R. Nitschke, *Nat. Chem.*, 2020, **12**, 270–275.
10 Z. Deng, W. Ying, K. Gong, Y.-J. Zeng, Y. Yan and X. Peng, *Small*, 2020, **16**, 1907016.
11 M. Gomes, L. Pison, C. Červinka and A. Padua, *Angew. Chem., Int. Ed.*, 2018, **57**, 11909–11912.
12 W. Shan, P. F. Fulvio, L. Kong, J. A. Schott, C. L. Do-Thanh, T. Tian, X. Hu, S. M. Mahurin, H. Xing and S. Dai, *ACS Appl. Mater. Interfaces*, 2018, **10**, 32–36.
13 S. He, L. Chen, J. Cui, B. Yuan, H. Wang, F. Wang, Y. Yu, Y. Lee and T. Li, *J. Am. Chem. Soc.*, 2019, **141**, 19708–19714.
14 B. Lai, J. Cahir, M. Y. Tsang, J. Jacquemin, D. Rooney, B. Murrer and S. L. James, *ACS Appl. Mater. Interfaces*, 2021, **13**, 932–936.
15 C. D. Gutsche, B. Dhawan, K. H. No and R. Muthukrishnan, *J. Am. Chem. Soc.*, 1981, **103**, 3782–3792.
16 S. Lim, H. Kim, N. Selvapalam, K. J. Kim, S. J. Cho, G. Seo and K. Kim, *Angew. Chem., Int. Ed.*, 2008, **47**, 3352–3355.
17 K. Jie, M. Liu, Y. Zhou, M. A. Little, A. Pulido, S. Y. Chong, A. Stephenson, A. R. Hughes, F. Sakakibara, T. Ogoshi, F. Blanc, G. M. Day, F. Huang and A. I. Cooper, *J. Am. Chem. Soc.*, 2018, **140**, 6921–6930.
18 (*a*) H. Kudo, R. Hayashi, K. Mitani, T. Yokozawa, N. C. Kasuga and T. Nishikubo, *Angew. Chem., Int. Ed.*, 2006, **45**, 7948–7952; (*b*) D. Shimoyama, R. Sekiya, H. Kudo and T. Haino, *Org. Lett.*, 2020, **22**, 352–356; (*c*) T. Nishikubo and H. Kudo, *Japan Patent*JP2008-280269A, 2008; (*d*) H. Yamada, T. Ikeda, T. Mizuta and T. Haino, *Org. Lett.*, 2012, **14**, 4510–4513; (*e*) D. Shimoyama, T. Ikeda, R. Sekiya and T. Haino, *J. Org. Chem.*, 2017, **82**, 13220–13230.
19 (*a*) N. Niina, H. Kudo and T. Nishikubo, *Chem. Lett.*, 2009, **38**, 1198–1199; (*b*) N. Niina, H. Kudo, K. Maruyama, T. Kai, T. Shimokawa, H. Oizumi, T. Itani and T. Nishikubo, *Polym. J.*, 2011, **43**, 407–413.
20 H. Kudo, Y. Suyama, H. Oizumi, T. Itani and T. Nishikubo, *J. Mater. Chem.*, 2010, **20**, 4445–4450.
21 S. R. Peerannawar and S. P. Gejji, *Comput. Theor. Chem.*, 2013, **1015**, 44–51.
22 Z. Zhai, C. Jiang, N. Zhao, W. Dong, H. Lan, M. Wang and Q. J. Niu, *J. Mater. Chem. A*, 2018, **6**, 21207–21215.
23 H. Kudo, D. Watanabe, T. Nishikubo, K. Maruyama, D. Shimizu, T. Kai, T. Shimokawa and C. K. Ober, *J. Mater. Chem.*, 2008, **18**, 3588–3592.
24 T. Nishikubo, H. Kudo, Y. Suyama, H. Oizumi and T. Itani, *J. Photopolym. Sci. Technol.*, 2009, **22**, 73–76.
25 J. Tian, P. K. Thallapally, S. J. Dalgarno, P. B. McGrail and J. L. Atwood, *Angew. Chem., Int. Ed.*, 2009, **48**, 5492–5495.
26 R. S. Patil, D. Banerjee, C. M. Simon, J. L. Atwood and P. K. Thallapally, *Chem.–Eur. J.*, 2016, **22**, 12618–12623.
27 D. Shimoyama, R. Sekiya, H. Maekawa, H. Kudo and T. Haino, *CrystEngComm*, 2020, **22**, 4740–4747. Note that the NMR spectrum reported in the ESI Fig. S1† may have inadvertently been incorrectly referenced and we suggest the correct chemical shifts are 1.12 ppm less than those reported.
28 A. Pohorille and L. R. Pratt, *J. Am. Chem. Soc.*, 1990, **112**, 5066–5074.